Prediction of Effective Elastic Properties of Carbon/UHMWPE Nanocomposites by Combination of Numerical and Analytical Modeling

STANISLAV BUKLOVSKYI[1], KATERYNA MIROSHNICHENKO[1], IGOR TSUKROV[1], REBECCA J. THOMSON[2], PEDER C. SOLBERG[2] and DOUGLAS W. VAN CITTERS[2]

ABSTRACT

In this paper, we investigate ultra-high-molecular-weight-polyethylene (UHMWPE) doped with conductive carbon black (CCB) nanoparticles. This nanocomposite is considered a candidate for biomedical applications such as orthopedics. Micro-computed tomography (μCT) and scanning electron microscopy studies show that the composite has a complex microstructure consisting of larger particles of UHMWPE surrounded by a thin layer containing a high concentration of CCB nano inclusions. The overall mechanical properties of these composites depend on the volume fraction of CCB and the manufacturing procedures e.g., compression molding or equal channel angular extrusion.

To predict the effective elastic properties of the CCB/UHMWPE nanocomposite, we propose a multiscale modeling framework based on a combined analytical-numerical approach. μCT images are processed to extract the size, shape, and orientation distributions of UHMWPE particles as well as the volume fractions and spatial distribution of CCB containing layer. These distributions are used to develop multiscale numerical models of the composite including finite element analysis of representative volume elements on the mesoscale, and micromechanical predictions of CCB containing layer on the microscale. The predictive ability of the models is confirmed by comparison with the experimental measurements obtained by dynamic mechanical analysis.

INTRODUCTION

In this paper, we model ultra-high-molecular-weight-polyethylene (UHMWPE) doped with conductive carbon black (CCB) nanoparticles. This nanocomposite is considered a candidate for biomedical applications such as orthopedics. UHMWPE is the articular surface material of choice for joint arthroplasties.

[1]University of New Hampshire, Durham, NH 03824, USA
[2]Dartmouth College, Hanover, NH 03755, USA

Previously, carbon fibers were combined with UHMWPE in an effort to increase strength and lower specific wear rates of surface materials [1]. These efforts turned out to be detrimental due to low levels of integration between the matrix and fibers, resulting in structural failures [2]. Contrary to carbon fibers, carbon nanoparticles can be successfully used with UHMWPE and as a coating for lubrication with other materials [3]. One of the advantages of CCB/UHMWPE composite is its potential to incorporate multifunctional behavior [4]. Conductive UHMWPE materials can be used to integrate mechanical and electrical sensors. In addition, it has been shown that the conductive properties of implant materials can be used to significantly reduce the number of bacteria present on the surface via electrochemical modes of action [5].

Micro-computed tomography (μCT) studies demonstrate that CCB/UHMWPE has a complex microstructure in which inclusions are not uniformly distributed in the material but rather concentrated at the boundaries around UHMWPE particles [6]. The composite consists of larger (~110μm) particles of UHMWPE surrounded by a thin (~10μm) layer containing a high concentration of CCB nano inclusions. Similar observations were made by Zhang et al. [7]. Fig.1 shows a typical CCB/UHMWPE μCT image. Black color corresponds to UHMWPE particles, while light grey color identifies regions of UHMWPE with high concentration of CCB (CCB-rich layer).

The complex microstructure of CCB/UHMWPE presents certain challenges for micromechanical modeling of its behavior. Most traditional analytical models are based on one-particle (Eshelby-type) solutions for inclusions uniformly distributed in the matrix material. [8]. Such models are not applicable for the considered microstructure, so a combined numerical-analytical multiscale approach has been chosen. First, μCT images are processed to extract the size, shape, and orientation distributions of UHMWPE particles as well as the volume fraction and spatial distribution of the CCB-containing layer. These distributions are then used to develop a finite element model of the representative volume element (RVE) of the composite (mesoscale). The properties of the CCB-containing layer (microscale) are determined with the micromechanical Mori-Tanaka formulas [9] utilizing the Eshelby tensor for spherical inclusions [10]. Note that a similar approach can be used for UHMWPE reinforced by nanographite [11] by approximating nanographite inclusion shapes as oblate spheroids and utilizing the

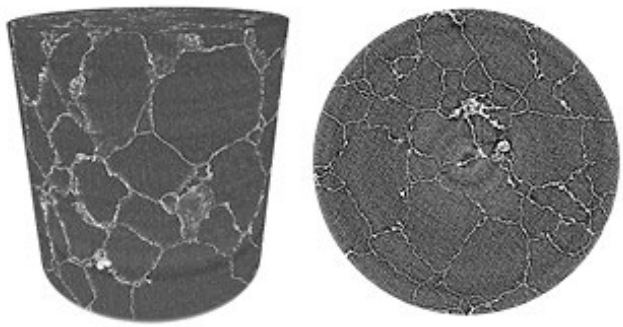

Figure 1. μCT image of CCB/UHMWPE composite with 1.5% weight fraction of CCB particles manufactured by compression molding.

corresponding components of the Eshelby tensor. In this paper, we present the numerical procedure to model CCB/UHMWPE on the mesoscale (scale of UHMWPE particles) and validate it by comparison with the experimental measurements.

DEVELOPMENT OF MESOSCALE MODELS

Mesoscale models were constructed for UHMWPE containing 0.5% wt., 1.0% wt., 2.5% wt., 5% wt., 7.5% wt., and 10% wt. of CCB. Statistics on the size, shape, and orientation distribution of UHMWPE particles were used to create synthetic microstructures in Dream3D open-source software [12]. Fig.2 illustrates the algorithm for producing synthetic microstructures. Two Dream3D pipelines were developed: Pipeline 1 was developed for the extraction of particles' size and shape. This pipeline uses thresholds to identify features on the image (UHMWPE particles), segments these features, and analyzes their size and shape. This data is exported as a CSV file with statistics on each feature. These statistics are then processed to find weighted (by volume) average size and shape characteristics. Pipeline 2 was developed to create a statistically similar microstructure using the processed statistics from Pipeline 1. This pipeline involves initializing a synthetic volume, establishing shape types, finding feature neighbors to match, and packing features in the RVE. The process results in a 3D model of the RVE, as illustrated in Fig.2c. The CCB-rich layer is introduced separately as follows: the Dream3D model of the RVE is exported to MATLAB as a structured VTK file. Then the interphase surfaces between UHMWPE particles are identified and the interphase domain is introduced by layer-by-layer reassigning the boundary voxels until the desired thickness of the interphase domain is achieved. An example of the resulting microstructure is shown in Fig. 2d. Development of the finite element mesh is performed in MATLAB utilizing Iso2Mesh [13] open-source software. The volumetric images serve as an input to internal Iso2mesh volumetric meshing procedure. The output of the procedure consists of an array of nodes and a tetrahedral mesh connectivity table with labels for UHMWPE and CCB-rich layer, respectively. This output mathematically represents a tetrahedral mesh. After the appropriate mesh reorientation and face mesh regeneration for cube's

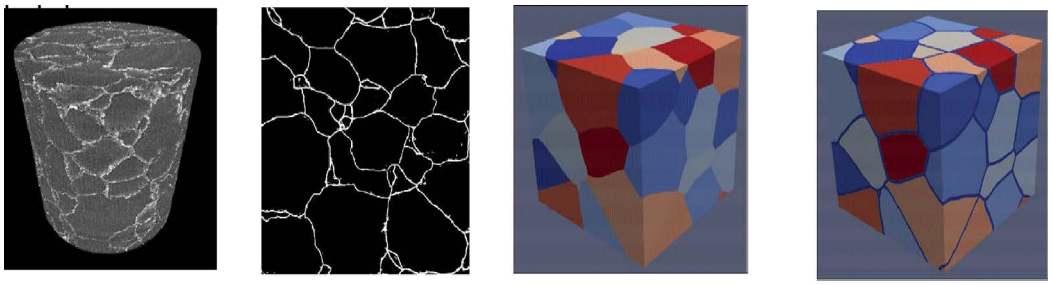

Figure 2. Synthetic microstructure reconstruction framework: (a) Raw μCT scan of carbon/UHMWPE composite, (b) Images processed via Dragonfly and MATLAB, (c) Synthetic microstructure of the composite, (d) Synthetic microstructure of the composite with additional interphase layer.

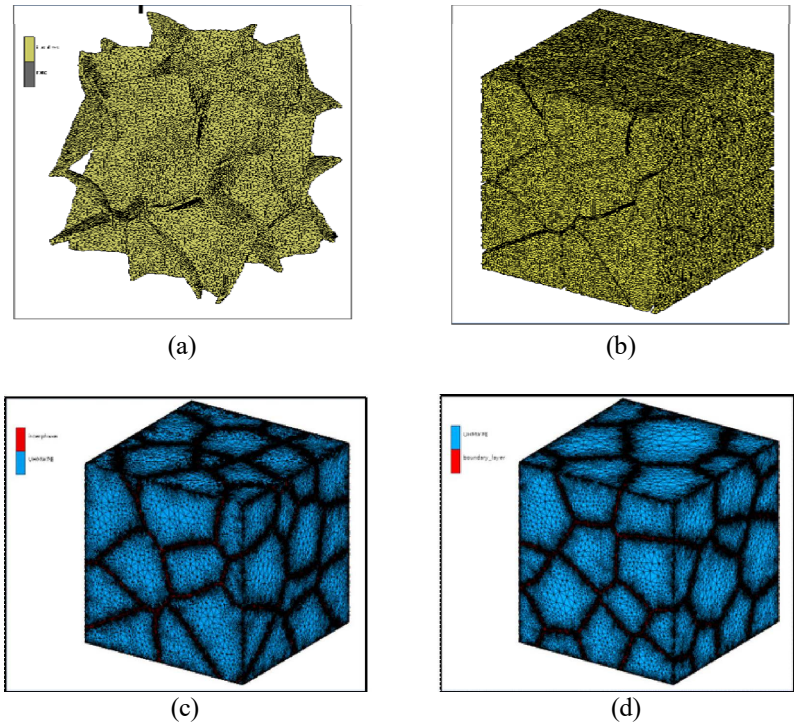

Figure 3. FEA mesh of CCB/UHMWPE RVE: (a) CCB-rich interphase, (b) UHMWPE particles, (c) first mesh realization, (d) second mesh realization.

faces, the mesh is ready for export to a commercial Hexagon Marc software for FEA analysis. Figs. 3a, b illustrate FE meshes of the interphase domain and UHMWPE particles; Figs. 3c, d show two realizations of the meshes utilized in this paper.

EFFECTIVE ELASTIC PROPERTIES OF CCB-RICH LAYER

It is assumed that CCB inclusions have a spherical shape and are randomly distributed in the CCB-rich layer. With this assumption, one of the traditional micromechanical schemes (Self-consistent, Mori-Tanaka, Differential) can be used to predict the effective properties of the layer. [8]. In this paper, the Mori-Tanaka scheme is utilized. The overall stiffness tensor $\boldsymbol{C}$ of the CCB-rich layer is expressed in terms of the stiffness of the matrix (UHMWPE) material $\boldsymbol{C}_m$ and stiffness of the inclusions (CCB) $\boldsymbol{C}_i$ as:

$$\boldsymbol{C} = \left(V_m \boldsymbol{C}_m + V_{c/L} \boldsymbol{C}_i : \boldsymbol{A}\right) : \left(V_m \boldsymbol{I} + V_{c/L} \boldsymbol{A}\right)^{-1} \quad (1)$$

where $\underline{\underline{\boldsymbol{I}}}$ is the 4th order identity tensor, subscripts *m* and *i* denote matrix and inclusions; $V_{c/L}$ and $V_m = 1 - V_{c/L}$ are the volume fractions of matrix and inclusions, respectively, $\boldsymbol{A}$ is the 4th order strain concentration tensor $\boldsymbol{A} = [\boldsymbol{I} + \boldsymbol{S} : (\boldsymbol{C}_m)^{-1} : (\boldsymbol{C}_i - \boldsymbol{C}_m)]^{-1}$, $\boldsymbol{S}$ is the Eshelby tensor for spherical inclusion, and the column is used to denote contraction of the 4th rank tensors over two internal indices.

The volume fraction of CCB ($V_{c/L}$) in the layer is determined based on the processing of μCT images. First, the volume fraction of CCB-rich layer is extracted (V_L). Then, it

is assumed that all CCB particles are located within the layer. (Note that this assumption is more accurate for compression molded composites while equal channel angular extrusion procedure might disperse some inclusions outside of the CCB-rich layer captured by μCT. See [14], [15] for description of the techniques). With this assumption, the volume fraction of CCB in the layer:

$$V_{c/L} = V_{CCB}/V_L \tag{2}$$

Table I presents the effective Young's and shear moduli of the CCB-rich layer for different weight fractions of CCB considered in this paper. The values are given with respect to the elastic properties of the neat material (E_{UH}, G_{UH}). The value of the Young's modulus for the neat UHMWPE was determined by the Dynamic Mechanical Analysis (DMA), which is described in the corresponding section of the paper.

CCB wt.%	$V_{c/L}$	**E/E$_{UH}$**	**G/G$_{UH}$**
0	0	1	1
0.5	0.32	1.95	1.98
1	0.33	1.99	2.03
2.5	0.46	2.73	2.79
5	0.57	3.68	3.78
7.5	0.61	4.16	4.28

TABLE I. Effective elastic properties of UHMWPE composite reinforced with CB inclusions.

NUMERICAL SIMULATIONS OF THE CCB-UHMWPE COMPOSITES

The effective elastic moduli of the composite were found numerically using the prescribed strain method. Six load cases applied to the RVE were considered, as shown in Table 2. In the table, $X_1^+, X_1^-, X_2^+, X_2^-, X_3^+, X_3^-$, denote the faces of the cube with outward normals directed in a positive or negative direction of the corresponding coordinate axes, a is the side length of the representative volume cube, $\varepsilon^{(0)}$ is the value of applied strain, u_1, u_2, u_3 are the displacements in x_1, x_2, x_3 directions, correspondingly. The resulting distributions of stresses were averaged over RVE and correlated with the applied strain to extract the overall material parameters. Simulations were conducted in a general purpose commercially available program Hexagon Marc.

Loadcase 1 (uniaxial tension in x_1 direction):

$X_1^- : u_1 = 0; \quad X_1^+ : u_1 = \varepsilon^{(0)} \cdot a;$

$X_1^-, X_1^+, X_2^-, X_2^+, X_3^-, X_3^+ : u_2 = 0; \quad u_3 = 0;$

Loadcase 2 (uniaxial tension in x_2 direction):

$X_2^- : u_2 = 0; \quad X_2^+ : u_2 = \varepsilon^{(0)} \cdot a;$

$X_1^-, X_1^+, X_2^-, X_2^+, X_3^-, X_3^+ : u_1 = 0; \quad u_3 = 0;$

Loadcase 3 (uniaxial tension in x_3 direction):
$X_3^- : u_3 = 0; \quad X_3^+ : u_3 = \varepsilon^{(0)} \cdot a;$
$X_1^-, X_1^+, X_2^-, X_2^+, X_3^-, X_3^+ : u_1 = 0; \quad u_2 = 0;$
Loadcase 4 (shear deformation in x_1x_2 plane):
$X_1^- : u_2 = 0; \quad X_1^+ : u_2 = \varepsilon^{(0)} \cdot a;$
$X_1^-, X_1^+, X_2^-, X_2^+, X_3^-, X_3^+ : u_1 = 0; \quad u_3 = 0;$
Loadcase 5 (shear deformation in x_2x_3 plane):
$X_2^- : u_3 = 0; \quad X_2^+ : u_3 = \varepsilon^{(0)} \cdot a;$
$X_1^-, X_1^+, X_2^-, X_2^+, X_3^-, X_3^+ : u_1 = 0; \quad u_2 = 0;$
Loadcase 6 (shear deformation in x_3x_1 plane):
$X_3^- : u_1 = 0; \quad X_3^+ : u_1 = \varepsilon^{(0)} \cdot a;$
$X_1^-, X_1^+, X_2^-, X_2^+, X_3^-, X_3^+ : u_2 = 0; \quad u_3 = 0;$

Table II. Load cases to determine the effective elastic parameters.

To extract and process Hexagon Marc numerical results, a custom MATLAB text processing procedure was developed. This procedure allows extraction of stress values from integration points of finite elements, extraction of nodes and their coordinates to calculate volumes of elements, and then volume averaging of stresses and strains in the RVE. These values are used to calculate the effective elastic moduli of the material as the proportionality coefficients between strains and stresses. Fig.4 illustrates distribution of σ_{11} stress in the RVE subjected to load case 1.

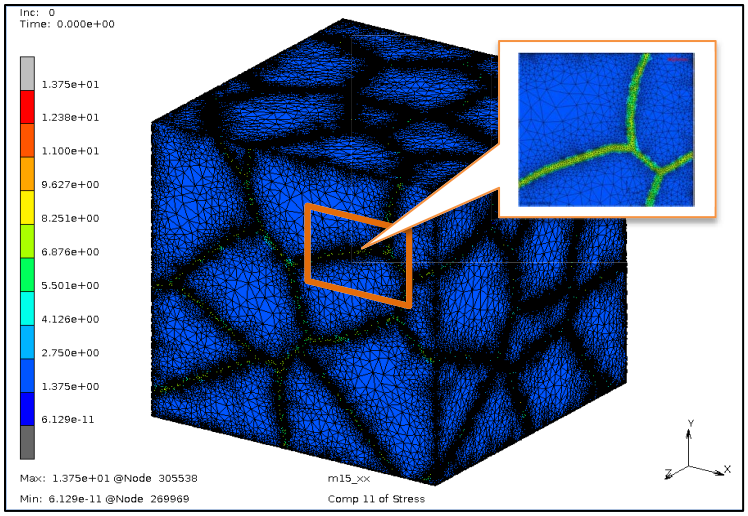

Figure 4. Distribution of σ_{11} stress in the RVE subjected to load case 1 (X, Y, Z axes correspond to x_1, x_2, x_3).

Note that the effective material is not ideally isotropic for each particular realization of the RVE. The effective isotropic elastic parameters were determined by averaging the values of the moduli in all directions. Variations in the predictions are quantified by the standard deviation error bars in Fig.5.

EXPERIMENTS TO DETERMINE THE YOUNG'S MODULUS OF THE MATERIAL

DMA was used to determine Young's modulus of neat GUR 1050 UHMWPE (input data) and CCB/UHMWPE composite (validation data). Both compression molded (CM) and equal channel angular extruded (ECAE) materials were tested. The 500 μm thick coupons were cut into 4.1 mm wide and 15 mm long samples. A Q800 DMA (TA Instruments, New Castle, DE) was used to analyze the loss and storage moduli of the composite CCB-UHMWPE samples. When placed in DMA clamps, the gauge lengths of the samples varied between 9 -12 mm. Thin film tension clamps were used to mount the samples in the DMA. After a five-minute isothermal equilibration time at 35°C, the samples were swept from 1 to 30 Hz by increasing the frequency to collect 40 data points. A strain of 0.2% oscillating was applied to the sample under 0.01 N of preload force. The storage moduli were reported at the highest value for each sample and averaged over 6 samples per composite.

Testing of the neat UHMWPE GUR 1050 determined the average tensile storage modulus $E' = 920\ MPa$ and tensile loss modulus $E'' = 37\ MPa$. These results show that for pure UHMWPE GUR 1050 the loss modulus can be neglected, and material's behavior can be considered purely elastic with elastic modulus $E = 920\ MPa$. This value can be combined with the known Poisson's ratio of 0.4 to evaluate the shear modulus of the neat UHMWPE $G = 330MPa$. The values of the Young's modulus for the CCB/UHMWPE composites determined with DMA are reported in the next section.

RESULTS AND DISCUSSION

Numerical estimates of the effective Young's and shear moduli are shown in Figs.5, 6. The estimates of the Young's modulus are compared with experimental measurements, obtained as described in the previous section and marked as blue and orange diamonds for CM and ECAP, correspondingly. It is observed that the numerical predictions lay within the confidence intervals of the measurements. As expected, the elastic moduli of the composite (both *E* and *G*) increase with the increase of concentration of stiff CCB particles. Note that the prediction for *E* at 15%wt. of CCB is shown to illustrate the trend in the increase in the Young's modulus. It is based on the assumption of perfect interface and load transfer which was not tested by experimental means. It is expected that the interface between nanoparticles and UHMWPE will eventually be compromised which will lead to the reduction in stiffness and strength with the increase of wt.% of CCB.

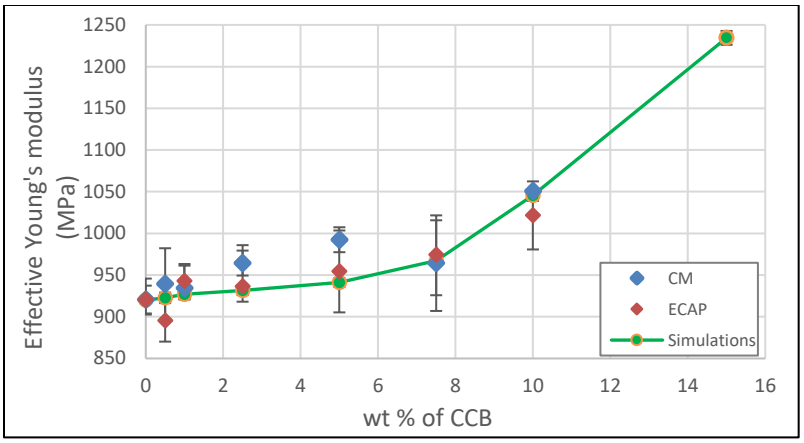

Figure 5. Numerical predictions and experimental measurements of the effective Young's modulus of CCB/UHMWPE composite.

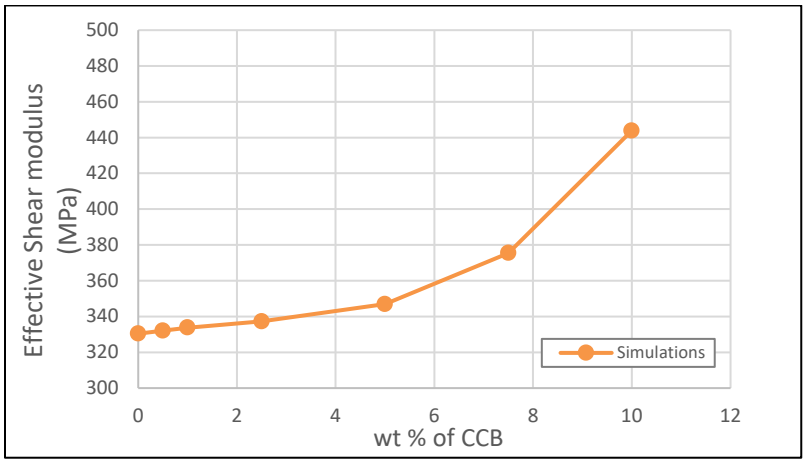

Figure 6. Numerical predictions of the shear modulus of CCB/UHMWPE composite.

CONCLUSIONS

A numerical procedure to predict the effective elastic properties of CCB/UHMWPE composite materials is proven to produce predictions for Young's modulus that are in good correspondence with the experimental measurements. The procedure is based on the μCT observed microstructure and incorporates information on concentration of CCB inclusions around UHMWPE particles. The assumptions (simplifications) of the uniform stiffness of CCB-rich layer and uniform distribution of CCB inclusions within the layer appear to be adequate for this mesoscale modeling effort that deals with the overall material behavior. Such assumptions might not be appropriate for fracture propagation and other local effects.

ACKNOWLEDGEMENTS

The authors acknowledge funding by the National Science Foundation EPSCoR award (#1757371)

REFERENCES

1. Baliga, B. R., Reddy, P., & Pandey, P. 2018. “Synthesis and Wear Characterization of CNF-UHMWPE Nanocomposites for Orthopaedic Applications,” *Mater. Today: Proceedings*, *5*(10), 20842–20848.
2. Thomson, Rebecca J., Limberg, Afton K., and Van Citters, Douglas W. 2023. "Nanoparticles in Joint Arthroplasties," *Nano LIFE* 13(01).
3. Rothammer, B., Marian, M., Neusser, K., Bartz, M., Böhm, T., Krauß, S., Schroeder, S., Uhler, M., Thiele, S., Merle, B., Kretzer, J. P., & Wartzack, S. 2021. “Amorphous Carbon Coatings for Total Knee Replacements—Part II: Tribological Behavior,” *Polymers 2021, 13*(11), p.1880.
4. Clark, A. C., Ho, S. P., & LaBerge, M. 2006. “Conductive composite of UHMWPE and CB as a dynamic contact analysis sensor,” Tribol. Int., *39*(11), pp.1327–1335.
5. Clark, C. M., Vishnoi, P., Swihart, M. T., & Ehrensberger, M. T. 2021. “The effect of cathodic voltage-controlled electrical stimulation of titanium on the surrounding microenvironment pH: An experimental and computational study,” Electrochim. Acta, *393*, 138853.
6. K. Miroshnichenko, S. Buklovskyi, K. Vasylevskyi, I. Tsukrov, H.J. Favreau, R. J. Thomson, P.C. Solberg, D.W. Van Citters. 2022. “Characterization and modeling of carbon black/ultra-high-molecular-weight-polyethylene nanocomposites manufactured with equal channel angular extrusion”, Proceedings of 20th International Conference on Fracture and Damage Mechanics, Malaga, Spain. 5-7 September, 2022.
7. Zhang, C., Ma, C. A., Wang, P., & Sumita, M. 2005. “Temperature dependence of electrical resistivity for carbon black filled ultra-high molecular weight polyethylene composites prepared by hot compaction,” *Carbon*, *43*(12), pp.2544–2553.
8. Eroshkin, O., & Tsukrov, I. 2005. “On micromechanical modeling of particulate composites with inclusions of various shapes,” Int. J. Solids Struct., *42*(2), pp.409–427.
9. Benveniste, Y. 1987. “A new approach to the application of Mori-Tanaka’s theory in composite materials,” Mech. Mater., *6*(2), pp.147–157.
10. Eshelby, J. D. 1957. “The Determination of the Elastic Field of an Ellipsoidal Inclusion, and Related Problems,” Proceedings of the Royal Society of London. Series A, Mathematical and Physical Sciences 241, 1226.
11. Favreau, H. J., Miroshnichenko, K. I., Solberg, P. C., Tsukrov, I. I., & van Citters, D. W. 2022. “Shear enhancement of mechanical and microstructural properties of synthetic graphite and ultra-high molecular weight polyethylene carbon composites,” J. Appl. Polym., *139*(20), 52175.
12. Groeber, M. A., & Jackson, M. A. 2014. “DREAM.3D: A Digital Representation Environment for the Analysis of Microstructure in 3D,” Integr. Mater. Manuf. 3(1) p.5
13. Fang, Q., Boas, D. A. 2009. “Tetrahedral mesh generation from volumetric binary and grayscale images,” Proceedings - 2009 IEEE International Symposium on Biomedical Imaging: From Nano to Macro, ISBI 2009, pp.1142–1145.
14. Cook, D. J., Chun, H. H., & van Citters, D. W. 2019. “Mechanical and Electrical Characterization of Two Carbon/Ultra High Molecular Weight Polyethylene Composites Created Via Equal Channel Angular Processing,” *J. Eng. Mater. Technol., Transactions of the ASME*, *141*(2), pp.1–7.
15. Vasylevskyi, K, Tsukrov I., Miroshnichenko K., Buklovskyi S., Grover H., and Van Citters D. 2021. “Finite Element Model of Equal Channel Angular Extrusion of Ultra High Molecular Weight Polyethylene,” J. Manuf. Sci. Eng. 143(12).